Science Advances

AAAS

advances.sciencemag.org/cgi/content/full/2/7/e1600500/DC1

Supplementary Materials for

Heterogeneity of cellular circadian clocks in intact plants and its correction under light-dark cycles

Tomoaki Muranaka and Tokitaka Oyama

Published 15 July 2016, *Sci. Adv.* **2**, e1600500 (2016)
DOI: 10.1126/sciadv.1600500

The PDF file includes:

- table S1. Summary of the quantitative analysis of cellular luminescence rhythms.
- Legends for movies S1 to S3
- Reference (*33*)

Other Supplementary Material for this manuscript includes the following:
(available at advances.sciencemag.org/cgi/content/full/2/7/e1600500/DC1)

- movie S1 (.mp4 format). Desynchronization of cellular luminescence rhythms on a frond under LL.
- movie S2 (.mp4 format). Desynchronization and damping of cellular luminescence rhythms on a frond under DD.
- movie S3 (.mp4 format). Asynchronous cellular luminescence rhythms on a frond under LL and their synchronization to LD cycles.

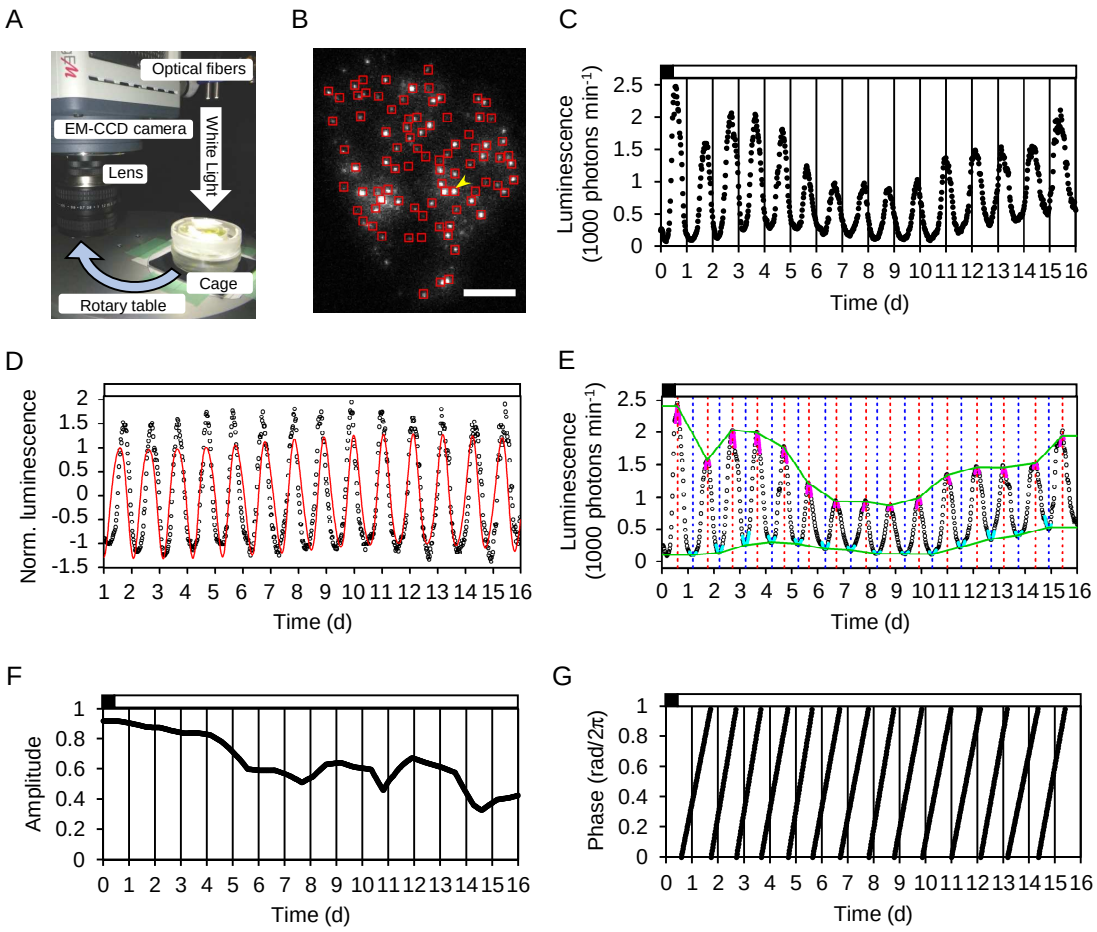

fig. S1. Outline of the quantitative analysis of cellular circadian rhythms. (**A**) Overview of the automated imaging system. A sample was set under the optical fibers and moved between under the optical fibers and under the camera lens every 30 min. (**B**) A bioluminescence image of the monitored frond (LDtoLL1, table S1) with ROI (red square; 6 × 6 pixels, pixel size ~ 25 μm) for luminescence quantification. Scale bar = 1 mm. (**C**) The luminescence intensity within the ROI indicated by the yellow arrow in B. (**D**) Result of FFT-NLLS analysis for the cellular luminescence rhythm displayed in C. The fitted multicomponent cosine function (red line) was drawn for the detrended and amplitude-normalized time series (open circle). (**E**) The result of peak/trough picking for the cellular rhythm displayed in C. The locally fitted quadratic-curves for peaks (magenta solid line) and troughs (cyan solid line), estimated PTs (red dashed line) and TTs (blue dashed line), and liner interpolation of peaks and troughs (green solid line) were drawn for the smoothed time series of C (open circle). (**F** and **G**) The amplitude (F) and phase (G) as a function of time were calculated from the results shown in E. Open and black bars indicate light and dark conditions, respectively.

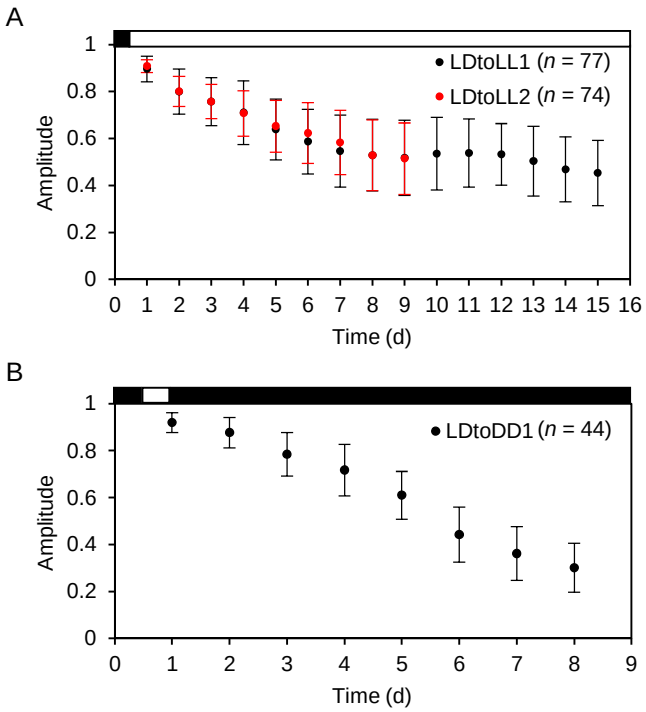

fig. S2. Temporal changes in amplitudes of cellular luminescence rhythms after release into LL or DD from LD. The mean ± SD of amplitudes of rhythm-sustained cells was plotted for each day after release into LL (**A**) or DD (**B**). Open and black bars indicate light and dark, respectively.

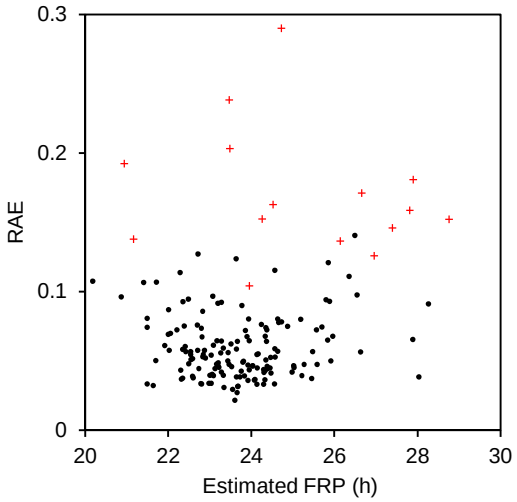

fig. S3. Results of FFT-NLLS analysis for cellular rhythms under LL. The RAE of rhythm-sustained cells (closed circles) and other cells that did not meet the criteria for circadian rhythms (red crosses) were plotted against the estimated FRPs for two replicate experiments (*n* = 167, days 1-9 of LDtoLL1-2, table S1).

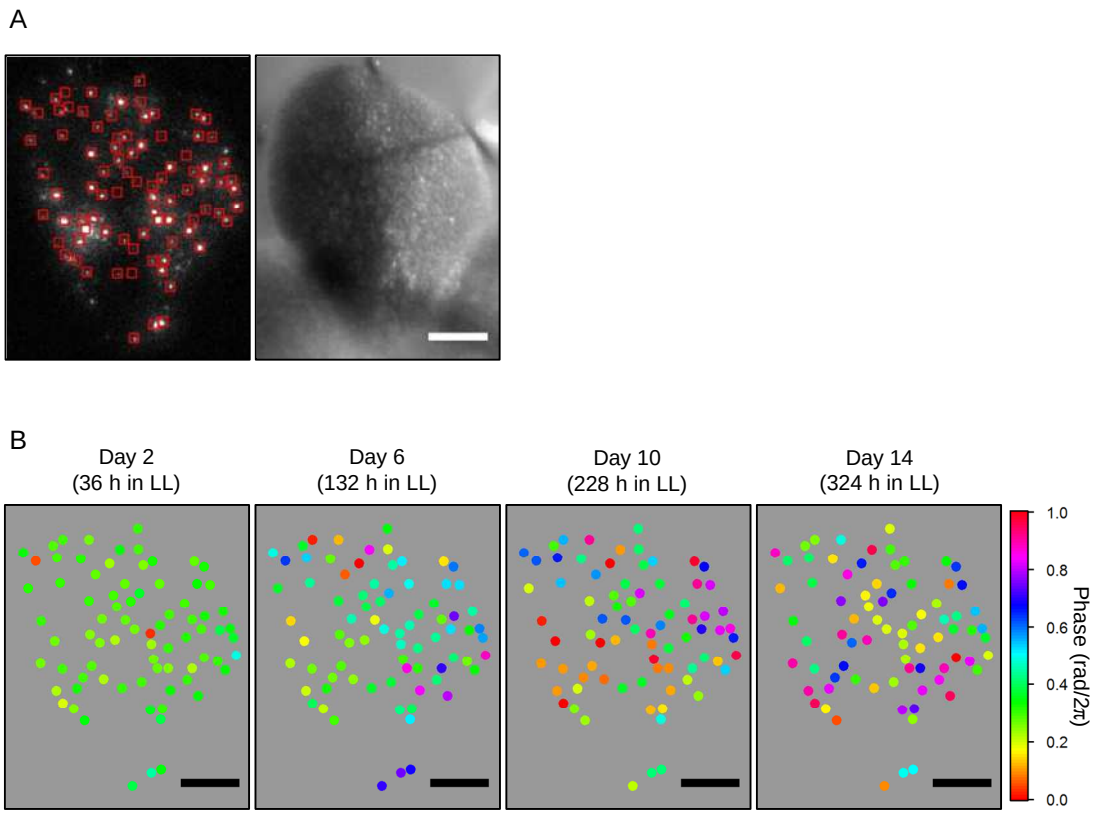

fig. S4. Time evolution of the spatial distribution of cellular circadian phases after release into LL from LD. (**A**) A bioluminescence (left) and a bright-field (right) image of the duckweed frond (LDtoLL1, table S1). (**B**) The spatial distribution of circadian phases of rhythm-sustained cells at each time point. Scale bars = 1 mm.

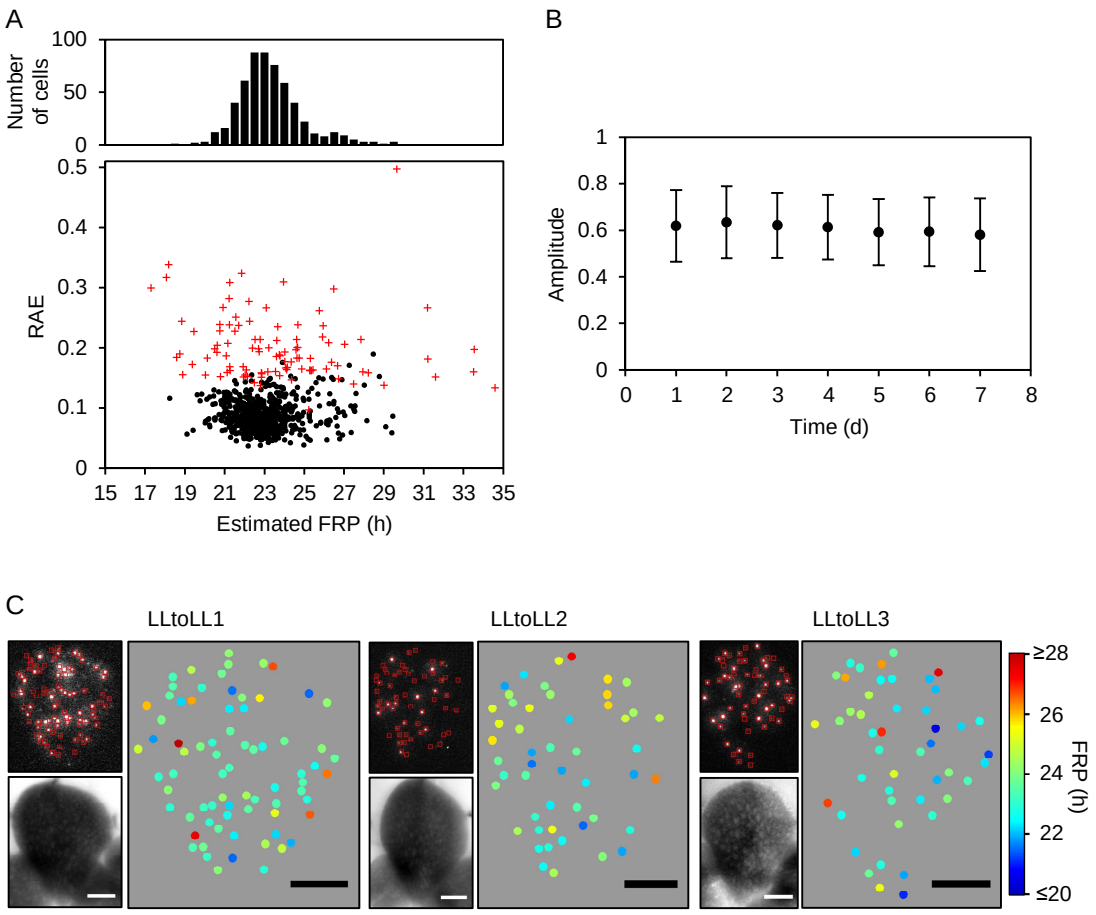

fig. S5. Characteristics of asynchronous cellular rhythms under LL. (**A**) Results of FFT-NLLS analysis for cellular rhythms in LL (LLtoLL1-9, *n* = 664, table S1). The RAE of rhythm-sustained cells (closed circle) and other cells that did not meet the criteria for circadian rhythms (red crosses) were plotted against the estimated FRPs. Histogram for estimated FRPs of rhythm-sustained cells is shown at the top. (**B**) Temporal changes of the amplitude of cellular rhythms in LL. The mean ± SD of rhythm-sustained cells of three replicate experiments (*n* = 171, LLtoLL1-3) were plotted for each day. (**C**) The spatial distribution of FRPs of rhythm-sustained cells of three replicate experiments (LLtoLL1-3). For each panel, a bioluminescence image (left-upper), a bright-field image (left-bottom), and a spatial distribution of circadian phases of rhythm-sustained cells (right) of each monitored frond are shown. Cellular FRPs were estimated by FFT-NLLS analysis. Scale bars = 1 mm.

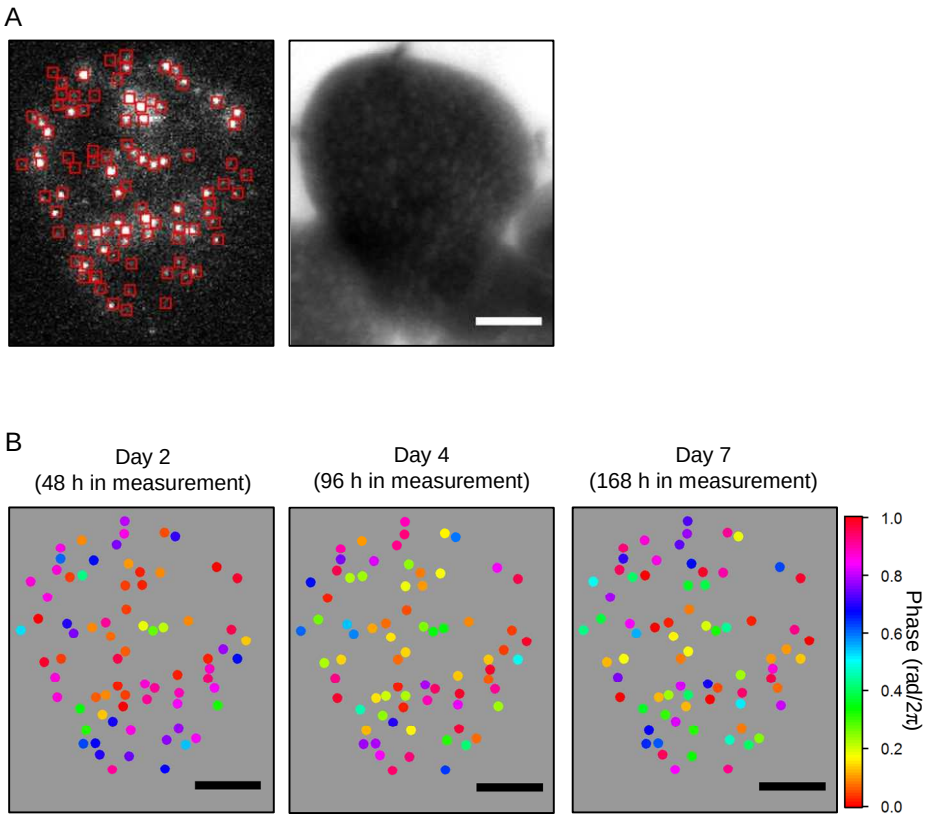

fig. S6. Time evolution of the spatial distribution of cellular circadian phases under LL. (**A**) A bioluminescence and a bright-field image of the monitored frond (LLoLL1, table S1). (**B**) Spatial distribution of the circadian phases of rhythm-sustained cells at each time point. Scale bars = 1 mm.

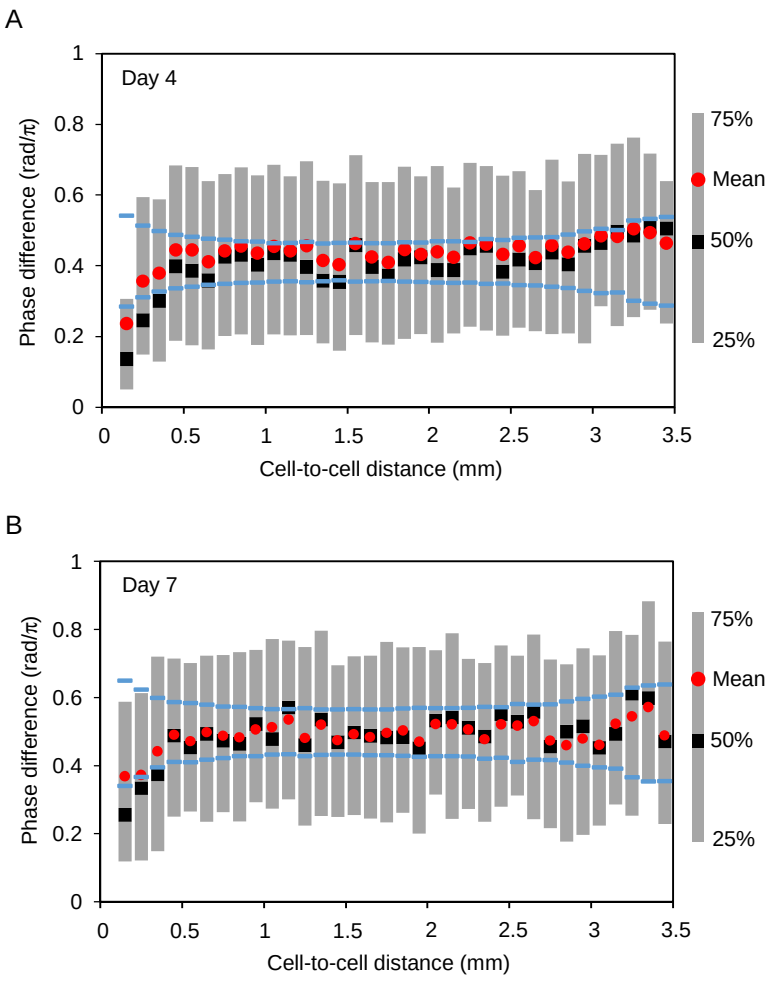

fig. S7. Relationship between phase differences between cellular rhythms and cell-to-cell distances. For all pairs of rhythm-sustained cells in each experiment (LLtoLL1-4 for day 4, LLtoLL1-3 for day 7, table S1), phase differences and cell-to-cell distances on day 4 (**A**) and day 7 (**B**) were calculated. Statistics of the phase differences were plotted at every 0.1 mm interval in cell-to-cell distances. Blue symbols at each cell-to-cell distance interval represent 95% confidence limits of median, assuming that samples in each interval have the same median value. The confidence limits were calculated based on resampling (10,000 repeats) from all samples.

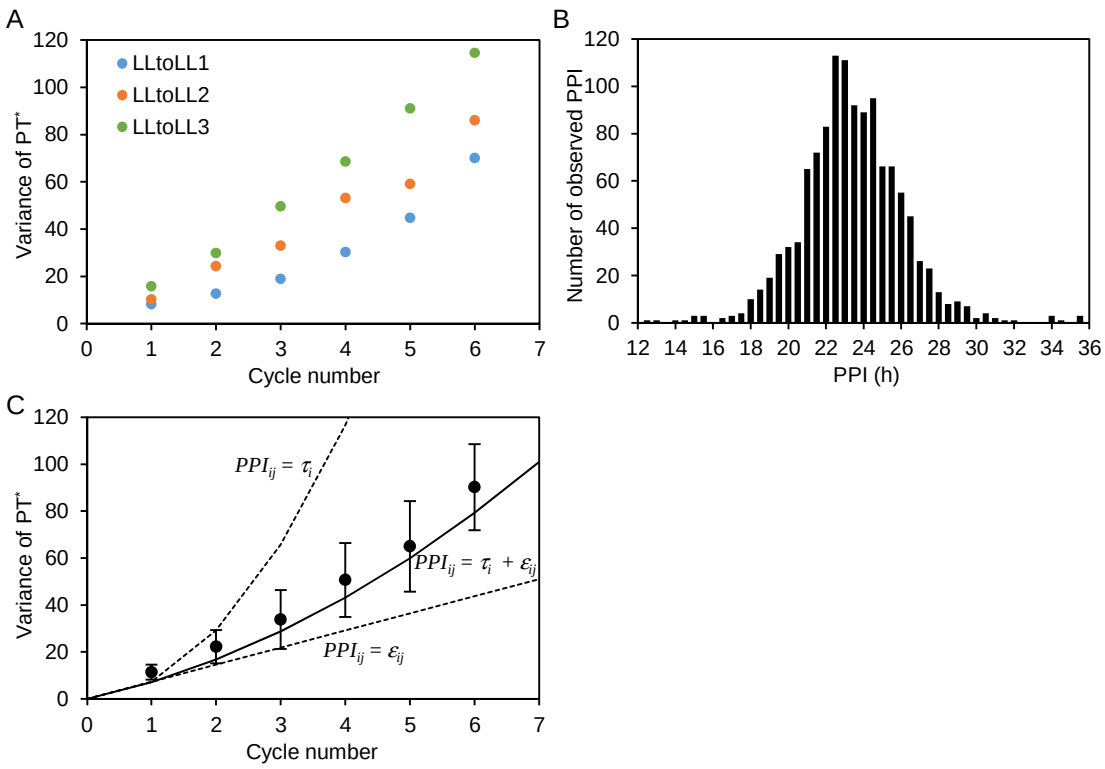

fig. S8. Population-level dynamics of cellular clocks explained by an ANOVA model. To analyze the population-level dynamics of cellular clocks, we evaluated the diffusion of PTs in data collected over 8 days of monitoring (LLtoLL1-3, table S1). We first converted the PT of each cell to PT* as $PT^*_{ij} = PT_{ij} - PT_{i1}$, where PT_{ij} is the jth PT of cell i. The across-cell variance of PT*, an index of diffusion of PT*s, increased cycle by cycle as shown in A. This increase in variance was due to the fact that the PPIs ranged widely as shown in B. We assumed that these PPIs were distributed as $PPI_{ij} = \tau_i + \varepsilon_{ij}$ (see text for detail). In this model, the variance of PT* during the nth cycle can be calculated as the function of SDs of τ_i and ε_{ij} (*33*). The calculated variance with estimated SDs followed the variance curve of PT* closely as shown in C ($r^2 = 0.73$). (**A**) The across-cell variance of PT* on each frond was plotted as a function of cycle number. (**B**) Histogram of observed PPIs (23.40 $\pm$ 2.67 h, mean $\pm$ SD, $n = 1212$). (**C**) The mean ± SD of the variance of PT* calculated from the three experiments and the simulated variance curve in statistical models were plotted as a function of cycle number. The variance of PT* on the nth cycle (V_n) was calculated from the following three models and parameter sets, $PPI_{ij} = \tau_i + \varepsilon_{ij}$ ($V_n = \sigma_\tau^2 n^2 + \sigma_\varepsilon^2 n$, $\sigma_\tau = 1.11$ h, $\sigma_\varepsilon = 2.45$ h), $PPI_{ij} = \tau_i$ ($V_n = \sigma_\tau^2 n^2$, $\sigma_\tau =$ 2.67 h), $PPI_{ij} = \varepsilon_{ij}$ ($V_n = \sigma_\varepsilon^2 n$, $\sigma_\varepsilon = 2.67$ h), where σ_τ and σ_ε represents SD of τ_i and ε_{ij}, respectively.

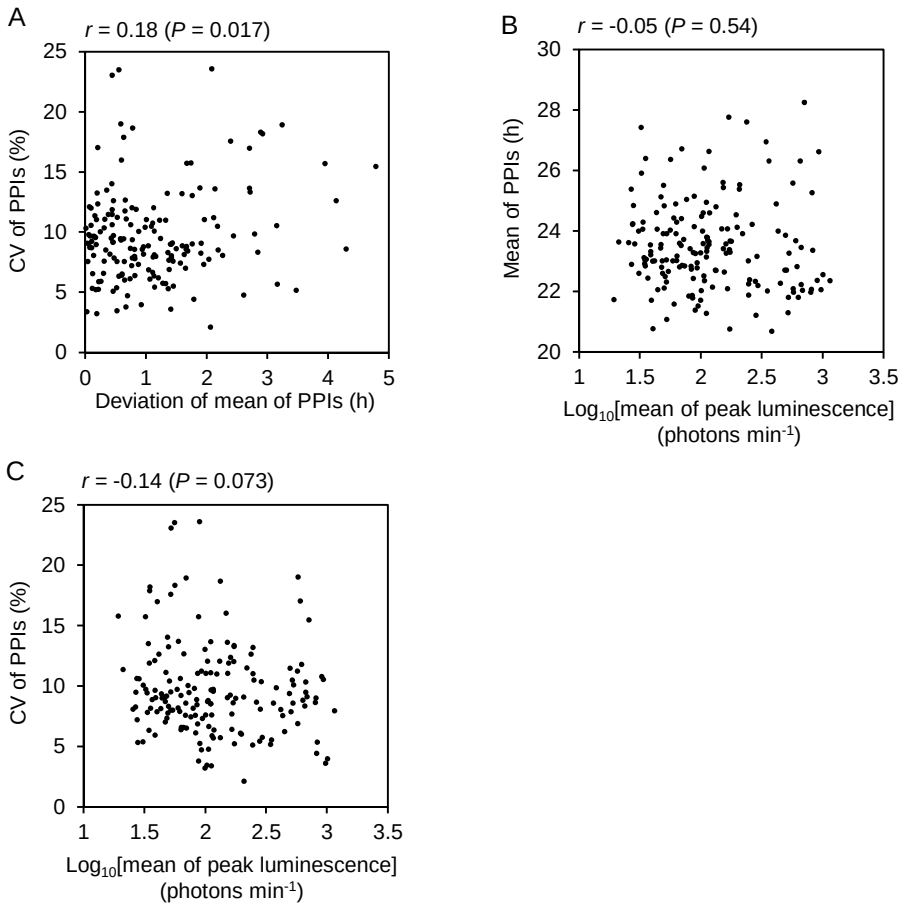

fig. S9. Correlation between characteristic parameters for cellular bioluminescence rhythms under LL. (**A**) Correlation between CV of PPIs and deviation in the mean of PPIs. (**B**) Correlation between mean of PPIs and mean of peak luminescence. (**C**) Correlation of CV of PPIs and mean of peak luminescence. Log scale was used for peak luminescence because cellular luminescence intensity varied over a wide range. The time series of rhythm-sustained cells based on data from 8 days of monitoring (n = 171, LLtoLL1-3, table S1) were used for this analysis.

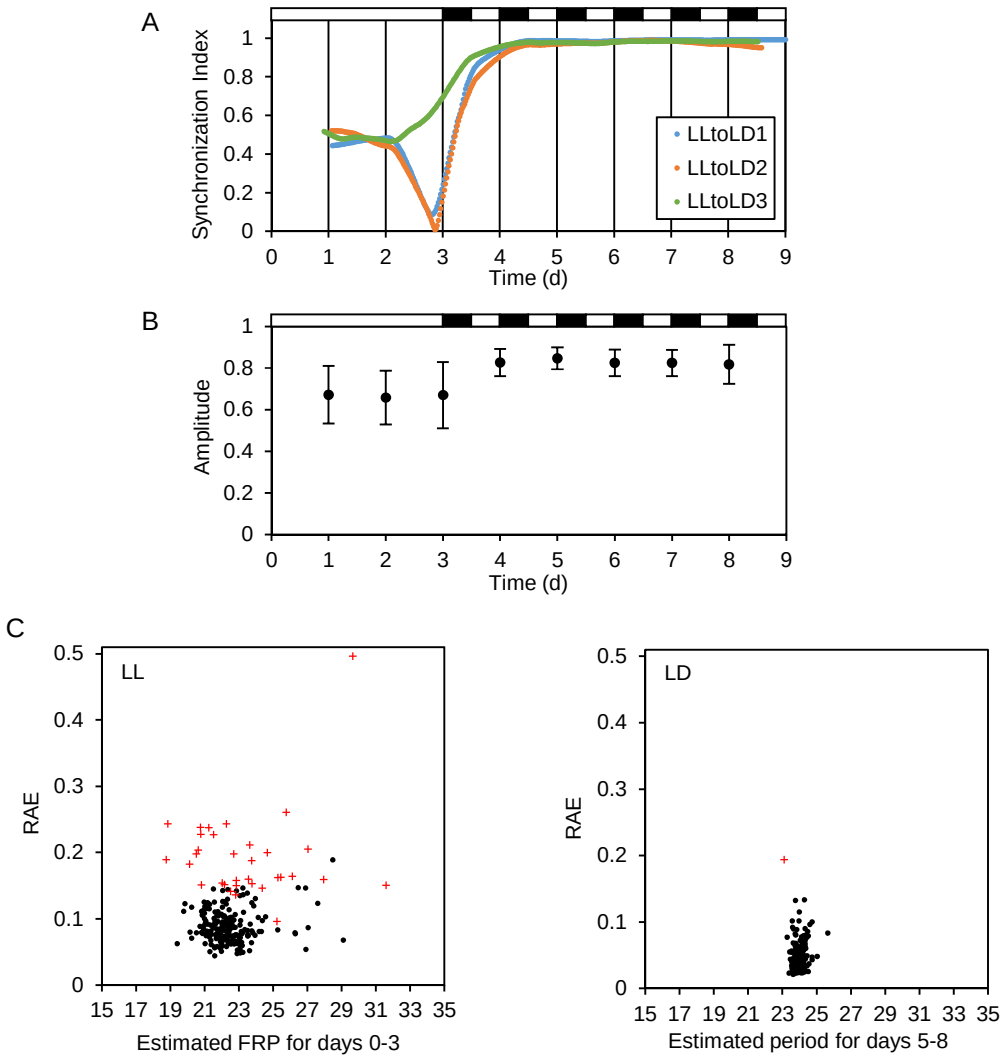

fig. S10. Cellular rhythms were synchronized to LD cycles within 2 days. Data from three experiments (LLtoLD1-3, table S1) were analyzed. (**A**) Temporal changes in synchronization index (SI) of three experiments. Before being subjected to LD, SI was 0.49 ± 0.01 (mean ± SD, n = 3, day 1.5). After being subjected to LD, SI increased to 0.98 ± 0.01 (mean ± SD, n = 3, day 5). The difference in traces of SI between LLtoLD1-2 and LLtoLD3 may reflect the differences in the distribution of cellular circadian phases at first light-dark transition (see also fig. S12B). (**B**) Temporal changes in amplitudes of cellular rhythms. The mean ± SD of rhythm-sustained cells was plotted for each day (n = 198). The amplitude increased rapidly after being subjected to LD. (**C**) Results of FFT-NLLS analysis for cellular rhythms in LL (left) and LD (right). The oscillation period varied in LL (22.4 ± 1.4 h, mean ± SD, n = 198) but was set to 24 h in LD (24.0 ± 0.3 h, mean ± SD, n = 231). Among three replicate experiments, mean of cellular FRPs in LL showed no significant difference (ANOVA, F = 2.4, P = 0.1). Open and black bars indicate light and dark, respectively.

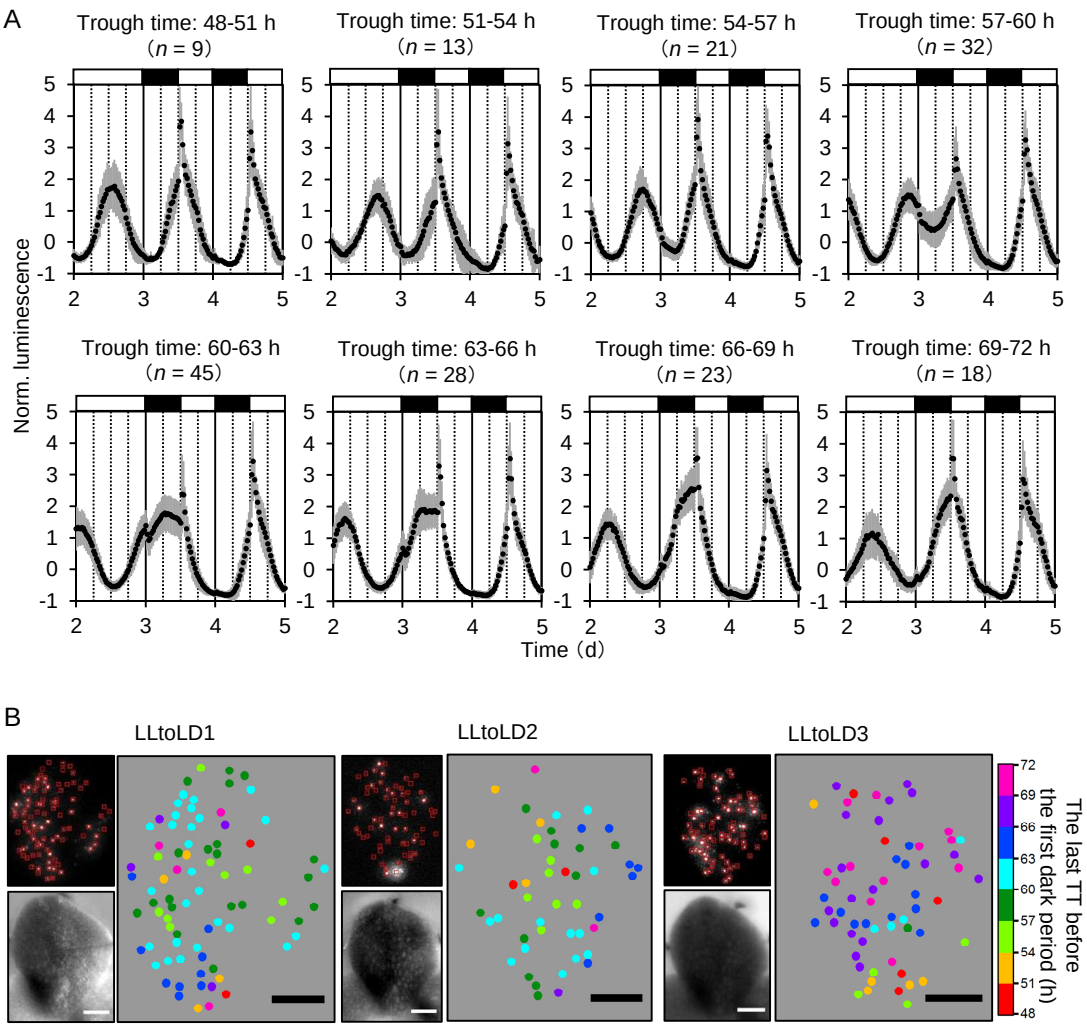

fig. S11. Cellular clocks respond to the first dark signal in a phase-dependent manner. (**A**) The phase-dependent response of cellular clocks to the first dark signal. The cellular rhythms of three experiments (LLtoLD1-3, table S1) were sorted into eight groups according to the last TTs before the first dark signal. For each group, the mean of their normalized luminescence was plotted (error bars = SD). Cellular rhythms were normalized by subtracting a 24 h moving average and dividing by the SD. To clarify the opposing behavior between two groups, TT: 57-60 h and TT: 60-63 h, TT was used as an index of phase because the last peaks before the first dark signal vanished in those two groups. Open and black bars indicate light and dark, respectively. (**B**) The spatial distribution of the last TTs before the first dark signal. For each panel, a bioluminescence image (left-upper), a bright-field image (left-bottom) and a spatial distribution of TTs (right) of each monitored frond are shown. Scale bars = 1 mm.

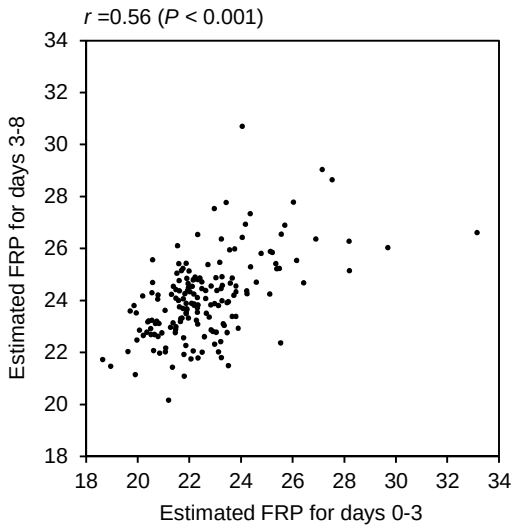

fig. S12. Correlation between FRPs during the first 3 days and during the subsequent 5 days. For rhythm-sustained cells monitored over 8 days (n = 171, LLtoLL1-3, table S1), FRPs during the first 3 days and those during the subsequent 5 days were estimated by FFT-NLLS. The positive correlation between them suggests that 3 days of monitoring is enough to estimate FRPs.

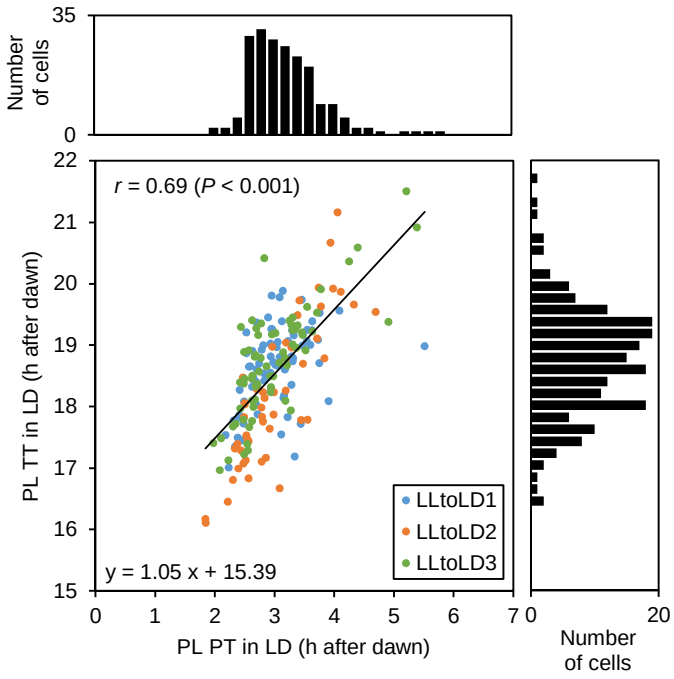

fig. S13. Locked phases under LD were significantly different among cells in a frond. Plot of PLTT against PLPT and their histograms for three experiments (LLtoLD1-3, table S1). As PLPTs and PLTTs, the mean of PTs and TTs during three days of LD (days 5.5-8.5) were used. The PLPTs showed significant variation among cellular clocks in each frond (ANOVA, LLtoLD1, $F = 9.9$, $P < 0.001$; LLtoLD2, $F = 4.6$, $P < 0.001$; LLtoLD3, $F = 6.0$, $P < 0.001$). The PLTTs also showed significant variation among cellular clocks in each frond (ANOVA, LLtoLD1, $F = 2.9$, $P < 0.001$; LLtoLD2, $F = 7.0$, $P < 0.001$; LLtoLD3, $F = 5.0$, $P < 0.001$). The positive correlation between PLPTs and PLTTs indicated that the observed variation of them reflects the variation in locked phases of cellular clocks in LD. The regression line for the combined data and its equation are shown.

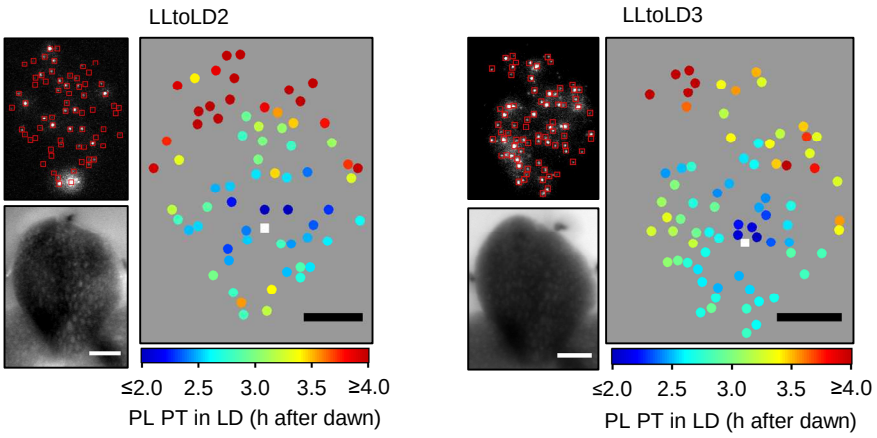

fig. S14. Spatial distribution of PLPTs under LD. For each panel, a bioluminescence image (left-upper), a bright-field image (left-bottom) and a spatial distribution of PLPTs in LD (right) of the monitored frond of two experiments (LLtoLD2-3, table S1) are shown. PLPT is represented as the mean of PTs during days 5.5-8.5. The center of a spatial pattern of PLPTs was estimated by quadric surface fitting and represented as a white square. Scale bars = 1 mm.

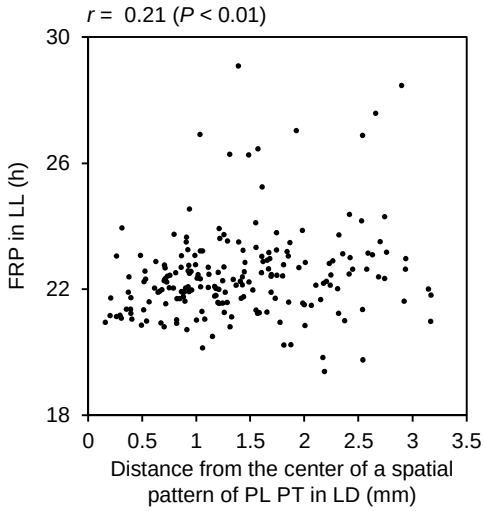

fig. S15. FRPs of cellular clocks showed no clear spatial patterns as PLPTs did. For rhythm-sustained cells of three experiments (LLtoLD1-3, table S1), FRPs in LL were plotted against distances from the estimated center of a spatial pattern of PLPTs in LD. The position of the estimated center for each experiment was displayed in Fig. 3D (LLtoLD1) and fig. S14 (LLtoLD2-3).

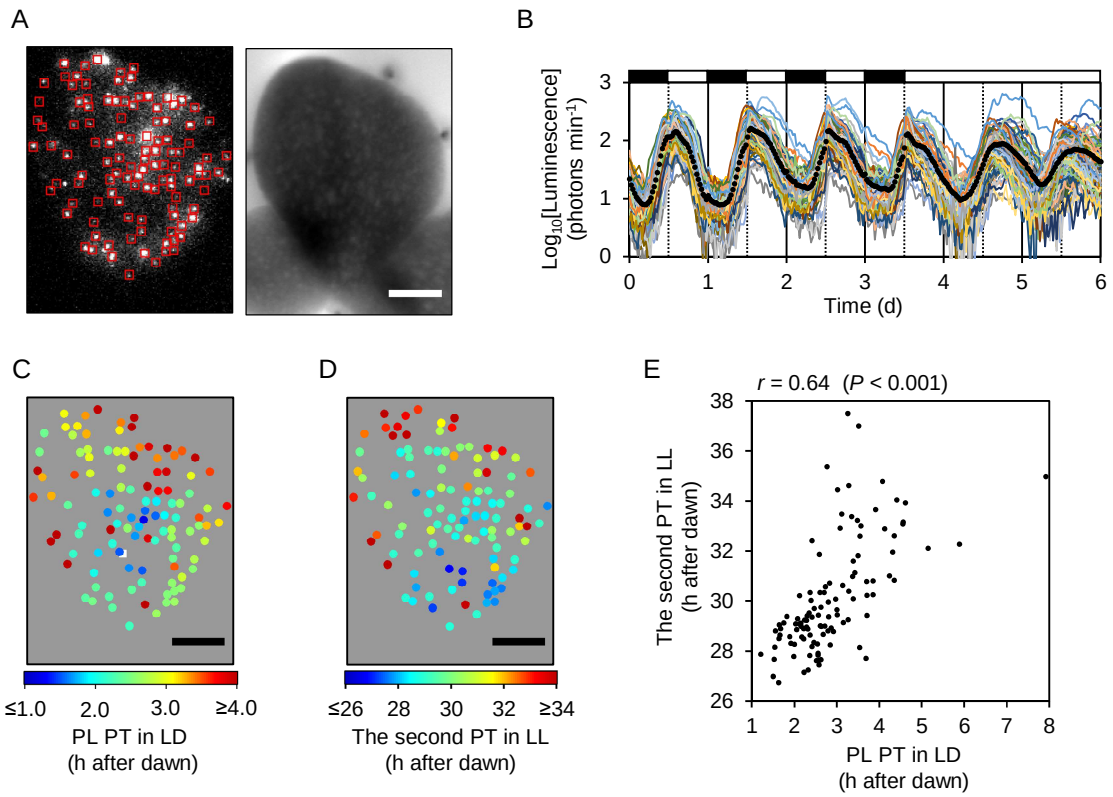

fig. S16. Spatial distribution of PLPTs after repeated LD cycles. Plants grown in LD for over a month were subjected to particle bombardment and then entrained in a cycle of LD before starting bioluminescence monitoring. (**A**) A bioluminescence (left) and bright-field (right) image of the monitored frond. (**B**) Luminescence traces (solid lines) and mean luminescence (closed circle) of 111 cells in the frond. Open and black bars indicate light and dark, respectively. (**C**) Spatial distribution of PLPTs in LD. PLPT was calculated as the mean of PTs during three days of growth in LD (days 1-4). The center of a spatial pattern of PLPTs was estimated by quadric surface fitting and represented as a white square. (**D**) Spatial distribution of the second PTs in LL. (**E**) The second PT in LL showed a positive correlation with PLPT in LD. Scale bars = 1 mm in A, C, D.

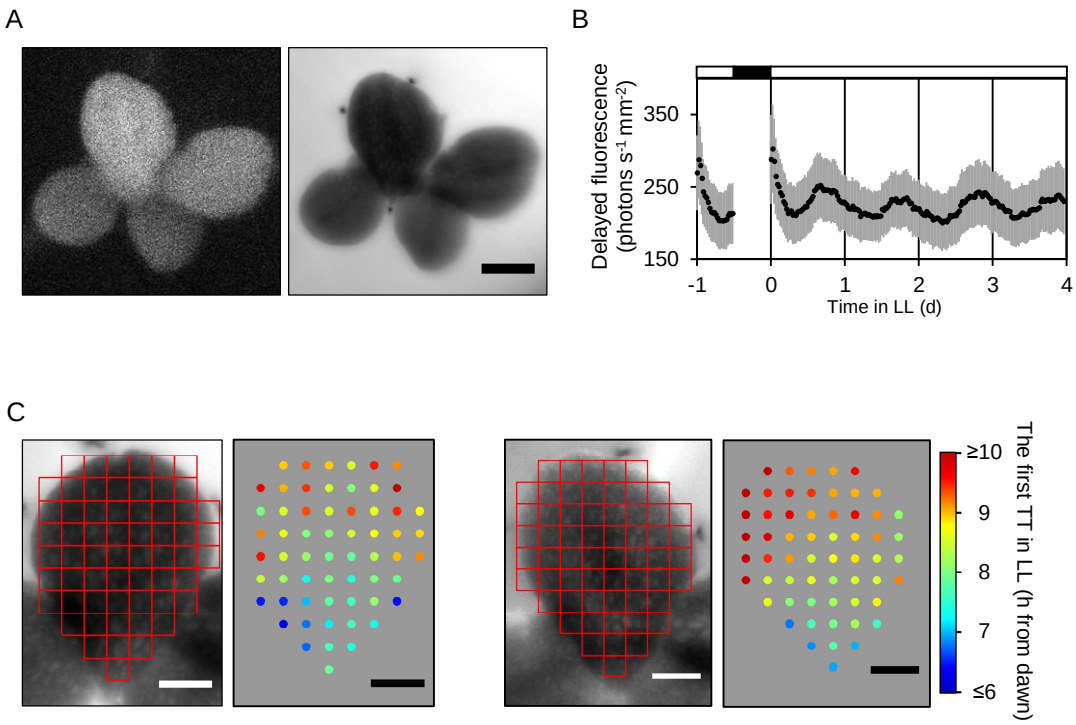

fig. S17. Spatial distribution of TTs of delayed fluorescence rhythms. Delayed fluorescence was monitored in LD for 3 days before switching to LL. (**A**) Delayed fluorescence and bright-field images of a colony of *L. gibba*. Scale bar = 2 mm. (**B**) Delayed fluorescence rhythm in LL after being released from LD. Mean of the signals within ROIs in the left panel of C was plotted. Error bars = SD. Open and black bars indicate light and dark, respectively. (**C**) Two examples of a spatial distribution of the first TT in LL. Scale bars = 1 mm.

table S1. Summary of the quantitative analysis of cellular luminescence rhythms.

Exp. index	Culture conditions	Preculture conditions after bombardment	Monitoring conditions	Number of measured cells	Analysis period (d)	Number of rhythm-sustained cells	Characteristic parameters of rhythm-sustained cells (mean ± SD)			
							Results of FFT-NLLS		Mean of PPIs (h)	CV of PPIs (%)
							Estimated period (h)	RAE		
LDtoLL1	LL	LD	LD to LL	85	1 – 16	78	24.5 ± 1.2	0.09 ± 0.04	24.2 ± 1.1	10.6 ± 4.6
					1 – 9	77	23.8 ± 1.3	0.06 ± 0.02	23.6 ± 1.2	7.3 ± 3.8
LDtoLL2	LL	LD	LD to LL	82	1 – 9	75	23.6 ± 1.4	0.06 ± 0.02	23.5 ± 1.4	7.2 ± 3.6
LDtoDD1	LL	LD	LD to DD	73	1 – 9	41	31.2 ± 1.7	0.09 ± 0.03	31.4 ± 2.2	12.3 ± 4.4
LLtoLL1	LL	LL	LL	89	0 – 8	74	23.7 ± 1.4	0.10 ± 0.03	23.5 ± 1.3	10.2 ± 4.0
LLtoLL2	LL	LL	LL	60	0 – 8	47	23.8 ± 1.4	0.09 ± 0.02	23.7 ± 1.5	9.5 ± 3.7
LLtoLL3	LL	LL	LL	60	0 – 8	46	23.4 ± 1.6	0.08 ± 0.03	23.3 ± 1.7	9.1 ± 3.6
LLtoLL4	LL	LL	LL	85	0 – 3	69	22.3 ± 1.8	0.09 ± 0.03	22.6 ± 2.0	9.3 ± 6.4
LLtoLL5	LL	LL	LL	76	0 – 3.5	71	23.2 ± 1.3	0.08 ± 0.02	23.0 ± 1.5	4.9 ± 2.5
LLtoLL6	LL	LL	LL	65	0 – 6	54	23.9 ± 1.7	0.08 ± 0.02	23.9 ± 1.7	7.6 ± 3.5
LLtoLD1	LL	LL	LL to LD	90	0 – 3[a]	80	22.2 ± 1.0	0.08 ± 0.02	22.1 ± 1.2	6.7 ± 5.7
					5 – 8	90	23.9 ± 0.2	0.04 ± 0.01	24.0 ± 0.2	1.3 ± 1.3
LLtoLD2	LL	LL	LL to LD	67	0 – 3[b]	51	22.7 ± 2.1	0.09 ± 0.03	22.7 ± 2.2	7.9 ± 6.4
					5 – 8	66	24.1 ± 0.3	0.06 ± 0.02	24.1 ± 0.4	3.4 ± 3.4
LLtoLD3	LL	LL	LL to LD	75	0 – 3[c]	68	22.6 ± 1.1	0.09 ± 0.02	22.7 ± 1.2	8.2 ± 5.6
					5 – 8	75	24.0 ± 0.2	0.05 ± 0.01	24.0 ± 0.3	2.5 ± 3.0

[a] analyzed as LLtoLL7
[b] analyzed as LLtoLL8
[c] analyzed as LLtoLL9

movie S1. Desynchronization of cellular luminescence rhythms on a frond under LL. Cellular luminescence recorded from the monitored frond during the experiment LDtoLL1 (Fig. 1B left, and table S1). A bright-field image of the monitored frond was inserted at the beginning of the movie. Time of measurement is displayed at the top-right. Light conditions were represented as squares at top-left; white and black boxes indicate light and dark, respectively.

movie S2. Desynchronization and damping of cellular luminescence rhythms on a frond under DD. Cellular luminescence recorded from the monitored frond during the experiment LDtoDD1 (Fig. 1B right, and table S1). Movie was created in the same manner as movie S1.

movie S3. Asynchronous cellular luminescence rhythms on a frond under LL and their synchronization to LD cycles. Cellular luminescence recorded from the monitored frond during the experiment LLtoLD1 (Fig. 3A and table S1). Movie was created in the same manner as movie S1.